nature nanotechnology

SUPPLEMENTARY INFORMATION
https://doi.org/10.1038/s41565-018-0145-8

In the format provided by the authors and unedited.

# Broadband, electrically tunable third-harmonic generation in graphene

**Giancarlo Soavi[1]*, Gang Wang[1], Habib Rostami[2], David G. Purdie[1], Domenico De Fazio[1], Teng Ma[1], Birong Luo[1], Junjia Wang[1], Anna K. Ott[1], Duhee Yoon[1], Sean A. Bourelle[1], Jakob E. Muench[1], Ilya Goykhman[1], Stefano Dal Conte[3,4], Michele Celebrano[4], Andrea Tomadin[2], Marco Polini[2], Giulio Cerullo[3,4] and Andrea C. Ferrari[1]***

[1]Cambridge Graphene Centre, University of Cambridge, Cambridge, UK. [2]Istituto Italiano di Tecnologia, Graphene Labs, Genova, Italy. [3]IFN-CNR, Milano, Italy. [4]Dipartimento di Fisica, Politecnico di Milano, Milano, Italy. *e-mail: gs544@cam.ac.uk; acf26@eng.cam.ac.uk

Supplementary Information for

# Broadband, electrically tuneable, third harmonic generation in graphene

Giancarlo Soavi[1], Gang Wang[1], Habib Rostami[2], David G. Purdie[1], Domenico De Fazio[1], Teng Ma[1], Birong Luo[1], Junjia Wang[1], Anna K. Ott[1], Duhee Yoon[1], Sean A. Bourelle[1], Jakob E. Muench[1], Ilya Goykhman[1], Stefano Dal Conte[3,4], Michele Celebrano[4], Andrea Tomadin[2], Marco Polini[2], Giulio Cerullo[3,4], Andrea C. Ferrari[1]

## S1 THG power dependence

Supplementary Fig.1 plots the experimental power dependence of THG as a function of incident power in double logarithmic scale. The slope is consistent with the cubic relation given by Eq.2 in the main text.

## S2 TGHE modeling

$\sigma^{(3)}_{\ell\ell\ell\ell}$ is calculated through a diagrammatic technique, with the light-matter interaction in the scalar potential gauge in order to capture all intra-, inter-band and mixed transitions [1–3]. We evaluate the diagram in Supplementary Fig.2 and denote by $\Pi^{(3)}_{\ell}$ the response function. $\hat{n}$ and $\hat{j}_\ell$ are the density and paramagnetic current operators. Then, $\sigma^{(3)}_{\ell\ell\ell\ell} = (ie)^3 \lim_{\vec{q}\to 0} \partial^3 \Pi^{(3)}_{\ell} / \partial q^3_{\ell}$, where $e > 0$ is the fundamental charge [2]. The Dirac Hamiltonian of low-energy carriers in SLG is $\mathcal{H}_{\rm k} = \hbar v_F \vec{k} \cdot \vec{\sigma}$ where $\vec{\sigma} = (\pm\sigma_x, \sigma_y)$ are the Pauli matrices in the sublattice basis. Note that $\pm$ represent the two valleys in the SLG Brillouin zone. We get $\sigma^{(3)}_{xxxx}(\omega, E_F, 0) = i\sigma^{(3)}_0 \bar{\sigma}^{(3)}_{xxxx}(\omega, E_F, 0)$ at $T_e = 0$ [1–3]:

$$\bar{\sigma}^{(3)}_{xxxx}(\omega, E_F, 0) = \frac{17G(2|E_F|, \hbar\omega_+) - 64G(2|E_F|, 2\hbar\omega_+)|}{24(\hbar\omega_+)^4} + \frac{45G(2|E_F|, 3\hbar\omega_+)}{24(\hbar\omega_+)^4} \tag{S1}$$

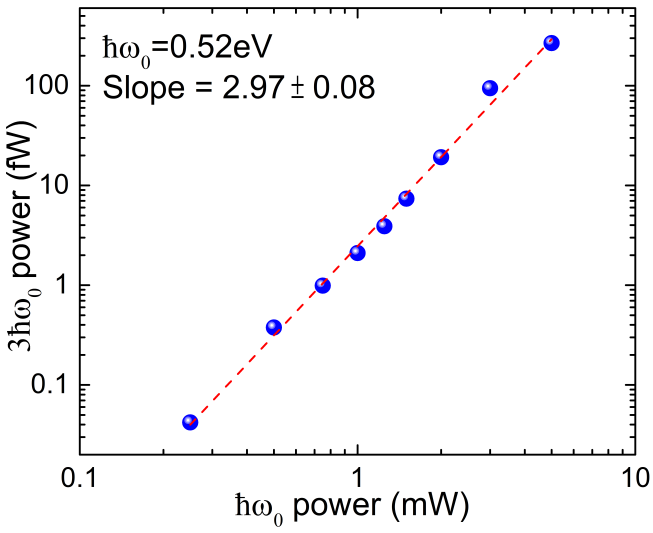


Supplementary Fig. 1. **THG power dependence**. THG power measured at $3\hbar\omega_0$=1.56eV as a function of the fundamental power measured at $\hbar\omega_0$=0.52eV. The slope∼3 is typical of the THG process, as for Eq.2 of the main text.

where $G(x,y) = \ln|(x+y)/(x-y)|$, $\sigma_0^{(3)} = N_f e^4 \hbar v_F^2/(32\pi)$ with $N_f = 4$ and $\hbar\omega_+ \equiv \hbar\omega + i0^+$. At finite $T_e$, $\sigma^{(3)}_{\ell\ell\ell\ell}$ is evaluated as [4]:

$$\sigma^{(3)}_{xxxx}(\omega, E_F, T_e) = \frac{1}{4k_B T_e}\int_{-\infty}^{\infty} dE\, \frac{\sigma^{(3)}_{xxxx}(\omega, E, 0)}{\cosh^2\left(\frac{E-\mu}{2k_B T_e}\right)}. \tag{S2}$$

### S2.1 THGE of SLG as an interface layer

In order to derive the THGE for SLG on a substrate we consider SLG as an interface layer between air and substrate [5,6], see Supplementary Fig.3, and implement electromagnetic boundary conditions for the non-harmonic radiations. The Maxwell equations in the nonlinear medium in the $m(\geq 2)$-th order of perturbation are given by [7,8]:

$$\vec{\nabla}\cdot\vec{B}^{(m)} = 0\ , \tag{S3}$$

$$\vec{\nabla}\cdot\vec{D}^{(m)} = \frac{\rho_f^{(m)}}{\epsilon_0} - \frac{1}{\epsilon_0}\vec{\nabla}\cdot\vec{P}^{(m)}\ , \tag{S4}$$

$$\vec{\nabla}\times\vec{E}^{(m)} = i\omega_\Sigma \vec{B}^{(m)}\ , \tag{S5}$$

$$\vec{\nabla}\times\vec{B}^{(m)} = \mu_0\vec{J}_f^{(m)} - i\frac{\omega_\Sigma}{c^2}\vec{D}^{(m)} - i\omega_\Sigma\mu_0\vec{P}^{(m)}\ . \tag{S6}$$

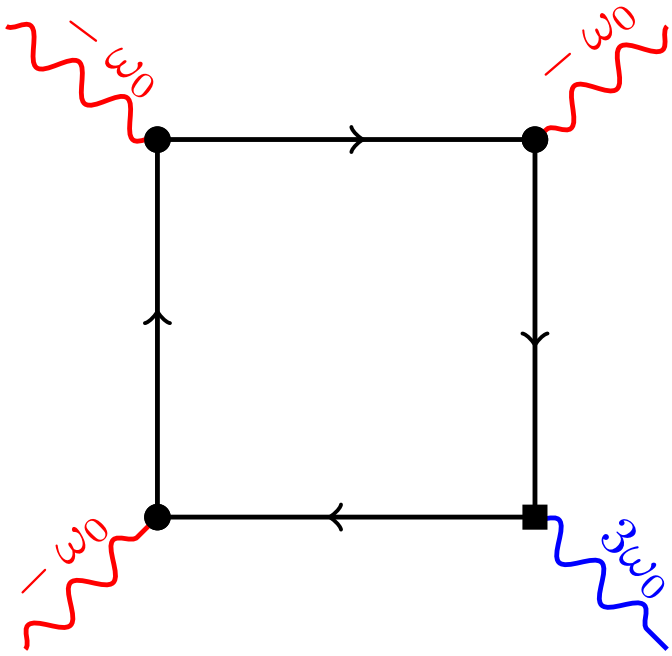


Supplementary Fig. 2. **Feynamn diagram for $\Pi_\ell^{(3)}$ in the scalar potential gauge**. Solid/wavy lines indicate non-interacting Fermionic propagators/external photons. Solid circles and square indicate density and current vertexes

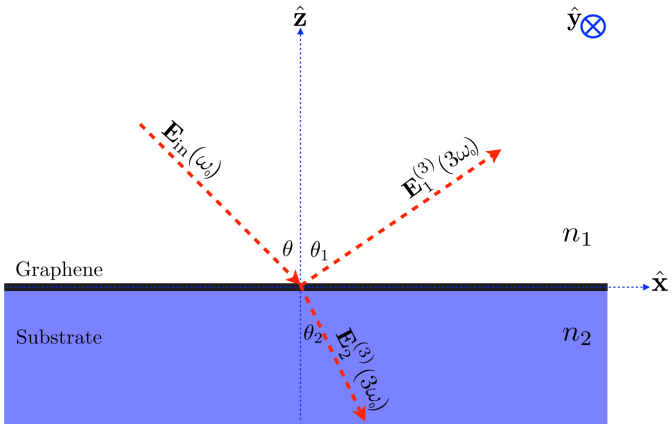


Supplementary Fig. 3. **Schematic of SLG on substrate**. The TH radiated waves in the top and bottom medium obey the TH Snell's law: $n_i(3\omega_0)\sin\theta_i = n_1(\omega_0)\sin\theta$. The red dashed arrows indicate the propagation direction of in-coming and out-going waves.

where $\vec{D}^{(m)} = \epsilon(\omega_\Sigma)\vec{E}^{(m)}$ is the *conventional* displacement vector. $\rho_f^{(m)}$ and $\vec{J}_f^{(m)}$ are the $m$-th order Fourier components of free charge and current. Note that $\omega_\Sigma = \sum_i^m \omega_i$, with $\omega_i$ the incoming photons frequency, with c and $\epsilon_0$ the speed of light and vacuum permittivity. For THG, we have $m = 3$, $\omega_{1,2,3} = \omega_0$ and $\omega_\Sigma = \omega_{THG} = 3\omega_0$. $\epsilon(\omega)$ is the isotropic and homogenous linear relative dielectric function. Only electric-dipole contributions are included.

We consider SLG in the $x$-$y$ plane embedded between air and a substrate. SLG is modeled by a dielectric function $\epsilon_s(\omega)$, nonlinear polarization, free surface charge and free surface current:

$$\vec{P}^{(m)} = \delta(z)\vec{\mathcal{P}}^{(m)} \ , \tag{S7}$$

$$\rho_f^{(m)} = \delta(z)\sigma_f^{(m)} \ , \tag{S8}$$

$$\vec{J}_f^{(m)} = \delta(z)\vec{K}_f^{(m)} \ . \tag{S9}$$

Having the Dirac delta, $\delta(z)$, in the above relations implies that SLG only shows up in the electromagnetic boundary conditions. Note that $\vec{\mathcal{P}}^{(m)}$ and $\vec{K}_f^{(m)}$ are in-plane vectors with zero component along the interface normal, $\hat{z}$. The interface layer is the only source of nonlinearity. We assume $\sigma_f^{(m)} = 0$ and $\vec{K}_f^{(m)} = 0$, consistent with our experiments, where there are no free surface charges and currents that oscillate at frequency $m\omega$ with $m = 2, 3, \ldots$.

The boundary conditions for the nonlinear fields at z=0 are obtained as:

$$\begin{aligned}
&\vec{B}_1^{(m)} - \vec{B}_2^{(m)} = \mu_0(\vec{K}_f^{(m)} - i\omega_\Sigma\vec{\mathcal{P}}^{(m)}) \times \hat{z} \ , \\
&\left\{\epsilon_1(\omega_\Sigma)\vec{E}_1^{(m)} - \epsilon_2(\omega_\Sigma)\vec{E}_2^{(m)}\right\} \cdot \hat{z} = \frac{\sigma_f^{(m)} - \vec{\nabla}_{2\mathrm{d}} \cdot \vec{\mathcal{P}}^{(m)}}{\epsilon_0} \ , \\
&(\vec{E}_1^{(m)} - \vec{E}_2^{(m)}) \times \hat{z} = 0 \ .
\end{aligned} \tag{S10}$$

Where the sub-indexes 1,2 stand for the top(bottom) medium and $\vec{\nabla}_{2d} = \hat{x}\partial/\partial x + \hat{y}\partial/\partial y$. The dielectric function of the interface layer, $\epsilon_s(\omega)$, does not emerge in the above boundary conditions.

The wave equation in the top and bottom media, with vanishing nonlinear polarization, follows:

$$\vec{\nabla} \times \vec{\nabla} \times \vec{E}^{(m)} - \frac{\omega_\Sigma^2}{c^2}\epsilon(\omega_\Sigma)\vec{E}^{(m)} = 0 \ . \tag{S11}$$

which has a plane wave solution [8]:

$$\vec{E}^{(m)} = \hat{\ell}\mathcal{E}^{(m)}e^{i(\vec{q}_\Sigma\cdot\vec{r} - \omega_\Sigma t)} + c.c. \tag{S12}$$

$\hat{\ell} \cdot \vec{q}_\Sigma = 0$ and the dispersion relation in the top and bottom media is:

$$q_\Sigma = |\vec{q}_\Sigma| = \frac{\omega_\Sigma}{c} n(\omega_\Sigma) \ . \tag{S13}$$

where $n(\omega_\Sigma) = \sqrt{\epsilon(\omega_\Sigma)}$ is the refractive index of the lossless media.

We consider a linearly polarized incident laser with arbitrary incident angle exposed to the interface layer:

$$\vec{E}_{in} = \{\hat{x}\mathcal{E}_x + \hat{y}\mathcal{E}_y + \hat{z}\mathcal{E}_z\} \, e^{i(\vec{q}\cdot\vec{r} - \omega_0 t)} + c.c. \tag{S14}$$

where

$$\vec{q} = \frac{\omega_0}{c} n_1(\omega_0)[-\cos\theta\hat{z} + \sin\theta\hat{x}] \ . \tag{S15}$$

The leading nonlinearity of SLG is encoded in $\overleftrightarrow{\sigma}^{(3)}$. Using the SLG symmetry, the third-order nonlinear polarization follows:

$$\vec{\mathcal{P}}^{(3)} = \vec{\widetilde{\mathcal{P}}}^{(3)} \exp\left\{ i\frac{3\omega_0}{c}\left[n_1(\omega_0)x\sin\theta - ct\right]\right\} + c.c. \tag{S16}$$

where

$$\begin{aligned}
\widetilde{\mathcal{P}}_x^{(3)} &= \frac{i}{3\omega_0}\sigma_{xxxx}^{(3)}\left\{\mathcal{E}_x^3 + \mathcal{E}_x\mathcal{E}_y^2\right\} \ , \\
\widetilde{\mathcal{P}}_y^{(3)} &= \frac{i}{3\omega_0}\sigma_{xxxx}^{(3)}\left\{\mathcal{E}_y^3 + \mathcal{E}_y\mathcal{E}_x^2\right\} \ , \\
\widetilde{\mathcal{P}}_z^{(3)} &= 0 \ .
\end{aligned} \tag{S17}$$

The wave-vectors of TH radiated waves in the top and bottom media are:

$$\begin{aligned}
\vec{q}_{3\omega_0,1} &= \frac{3\omega_0}{c} n_1(3\omega_0)[\cos\theta_1\hat{z} + \sin\theta_1\hat{x}] \ , \\
\vec{q}_{3\omega_0,2} &= \frac{3\omega_0}{c} n_2(3\omega_0)[-\cos\theta_2\hat{z} + \sin\theta_2\hat{x}] \ .
\end{aligned} \tag{S18}$$

According to the boundary condition relations of Eq.S10, we find $q_{3\omega_0,1,x} = q_{3\omega_0,2,x} = 3q_x$. Therefore, we derive the Snell's law for THG:

$$n_2(3\omega_0)\sin\theta_2 = n_1(3\omega_0)\sin\theta_1 = n_1(\omega_0)\sin\theta \ . \tag{S19}$$

Considering the refractive indexes frequency dependence, the Snell's law for THG implies that $\sin\theta_1 = [n_1(\omega_0)/n_1(3\omega_0)]\sin\theta$ is not generally equal to $\sin\theta$, in contrast with the specular reflection for first harmonic generation [8].

The plane wave nature of the TH radiations implies:

$$\cos\theta_1 \mathcal{E}^{(3)}_{1,z} + \sin\theta_1 \mathcal{E}^{(3)}_{1,x} = 0 \ ,$$
$$-\cos\theta_2 \mathcal{E}^{(3)}_{2,z} + \sin\theta_2 \mathcal{E}^{(3)}_{2,x} = 0 \ . \tag{S20}$$

By considering Eqs.S17,S18, the boundary condition relations Eq.S10 become:

$$n_1(3\omega_0)\left[\cos\theta_1 \mathcal{E}^{(3)}_{1,x} - \sin\theta_1 \mathcal{E}^{(3)}_{1,z}\right] +$$
$$n_2(3\omega_0)\left[\cos\theta_2 \mathcal{E}^{(3)}_{2,x} + \sin\theta_2 \mathcal{E}^{(3)}_{2,z}\right] = i\frac{3\omega_0}{c}\frac{\widetilde{\mathcal{P}}_x}{\epsilon_0} \ , \tag{S21}$$

$$n_1(3\omega_0)\cos\theta_1 \mathcal{E}^{(3)}_{1,y} + n_2(3\omega_0)\cos\theta_2 \mathcal{E}^{(3)}_{2,y} = -i\frac{3\omega_0}{c}\frac{\widetilde{\mathcal{P}}_y}{\epsilon_0} \ , \tag{S22}$$

$$n_1(3\omega_0)\sin\theta_1 \mathcal{E}^{(3)}_{1,y} - n_2(3\omega_0)\sin\theta_2 \mathcal{E}^{(3)}_{2,y} = 0 \ , \tag{S23}$$

$$\mathcal{E}^{(3)}_{1,x} = \mathcal{E}^{(3)}_{2,x} \ , \tag{S24}$$

$$\mathcal{E}^{(3)}_{2,y} = \mathcal{E}^{(3)}_{2,y} \ , \tag{S25}$$

$$n_1(3\omega_0)^2 \mathcal{E}^{(3)}_{1,z} - n_2(3\omega_0)^2 \mathcal{E}^{(3)}_{2,z} = -i\frac{3\omega_0}{c}\frac{\widetilde{\mathcal{P}}_x}{\epsilon_0} n_1(\omega_0)\sin\theta \ . \tag{S26}$$

From Eqs.S21-S26,S19,S20 we get:

$$\mathcal{E}^{(3)}_{i,x} = S_{i,x}\frac{\sigma^{(3)}_{xxxx}}{c\epsilon_0}\left\{\mathcal{E}_x^3 + \mathcal{E}_x\mathcal{E}_y^2\right\} \ , \tag{S27}$$

$$\mathcal{E}^{(3)}_{i,y} = S_{i,y}\frac{\sigma^{(3)}_{xxxx}}{c\epsilon_0}\left\{\mathcal{E}_y^3 + \mathcal{E}_y\mathcal{E}_x^2\right\} \ , \tag{S28}$$

$$\mathcal{E}^{(3)}_{i,z} = S_{i,z}\frac{\sigma^{(3)}_{xxxx}}{c\epsilon_0}\left\{\mathcal{E}_x^3 + \mathcal{E}_x\mathcal{E}_y^2\right\} \ . \tag{S29}$$

where

$$S_{1,x} = S_{2,x} = -\frac{\cos\theta_1\cos\theta_2}{n_1(3\omega_0)\cos\theta_2 + n_2(3\omega_0)\cos\theta_1} \ , \tag{S30}$$

$$S_{1,y} = S_{2,y} = -\frac{1}{n_1(3\omega_0)\cos\theta_2 + n_2(3\omega_0)\cos\theta_1} \ , \tag{S31}$$

$$S_{1,z} = \frac{\cos\theta_2\sin\theta_1}{n_1(3\omega_0)\cos\theta_2 + n_2(3\omega_0)\cos\theta_1} \ , \tag{S32}$$

$$S_{2,z} = -\frac{\cos\theta_1\sin\theta_2}{n_1(3\omega_0)\cos\theta_2 + n_2(3\omega_0)\cos\theta_1} \ . \tag{S33}$$

For normal incidence we have $\theta = 0$. From Eq.S19 we have $\theta_1 = \theta_2 = 0$. Therefore, $S_{i,z} = 0$ and $S_{i,x} = S_{i,y} = -1/[n_1(3\omega_0) + n_2(3\omega_0)]$. The time-average of the incident intensity gives $I_{\omega_0} = 2n_1(\omega_0)\epsilon_0 c|\vec{E}_{in}|^2$. The intensity of the transmitted TH signal is $I_{3\omega_0} = 2n_2(3\omega_0)\epsilon_0 c|\vec{E}^{(3)}|^2$. From this we get Eq.2 of the main text for THGE.

### S2.2 Symmetry considerations

The rank-4 tensor of $\sigma^{(3)}$ transforms as follows under an arbitrary $\phi$-rotation:

$$\sigma^{(3)}_{\alpha'\beta'\gamma'\delta'} = \sum_{\alpha\beta\gamma} R_{\alpha'\alpha}(\phi)R_{\beta'\beta}(\phi)R_{\gamma'\gamma}(\phi)R_{\delta'\delta}(\phi)\sigma^{(3)}_{\alpha\beta\gamma\delta} \ . \tag{S34}$$

We take the $z$-axis as the rotation-axis, perpendicular to SLG. Therefore, the rotation tensor is:

$$\overleftrightarrow{R}(\phi) = \begin{pmatrix} \cos\phi & \sin\phi \\ -\sin\phi & \cos\phi \end{pmatrix} \ . \tag{S35}$$

We take $\hat{\ell} = \overleftrightarrow{R}(\phi) \cdot \hat{x}$. By plugging Eq.S35 in S34, we get:

$$\begin{aligned}
\sigma^{(3)}_{\ell\ell\ell\ell} &= [\sin\phi]^4\sigma^{(3)}_{yyyy} + [\cos\phi]^4\sigma^{(3)}_{xxxx} \\
&+ \cos\phi[\sin\phi]^3\left[\sigma^{(3)}_{xyyy} + \sigma^{(3)}_{yxyy} + \sigma^{(3)}_{yyxy} + \sigma^{(3)}_{yyyx}\right] \\
&+ [\cos\phi]^3\sin\phi\left[\sigma^{(3)}_{xxxy} + \sigma^{(3)}_{xxyx} + \sigma^{(3)}_{xyxx} + \sigma^{(3)}_{yxxx}\right] \\
&+ [\cos\phi\sin\phi]^2\left[\sigma^{(3)}_{xxyy} + \sigma^{(3)}_{xyxy} + \sigma^{(3)}_{xyyx}\right. \\
&\left.+ \sigma^{(3)}_{yxxy} + \sigma^{(3)}_{yxyx} + \sigma^{(3)}_{yyxx}\right].
\end{aligned} \tag{S36}$$

Because of the $C_{6v}$ symmetry for SLG on a substrate, there are only 4 independent tensor elements [7]:

$$\begin{aligned}
&\sigma^{(3)}_{xxxx} = \sigma^{(3)}_{yyyy} = \sigma^{(3)}_{xxyy} + \sigma^{(3)}_{xyyx} + \sigma^{(3)}_{xyxy} \\
&\sigma^{(3)}_{xxyy} = \sigma^{(3)}_{yyxx}, \\
&\sigma^{(3)}_{xyyx} = \sigma^{(3)}_{yxxy}, \\
&\sigma^{(3)}_{xyxy} = \sigma^{(3)}_{yxyx}.
\end{aligned} \tag{S37}$$

By implementing Eq. S37 in Eq.S36, we get $\sigma^{(3)}_{\ell\ell\ell\ell} = \sigma^{(3)}_{xxxx}$.

### S2.3 Effect of finite relaxation rate

The effect of finite $\tau$ in the TH conductivity can be derived from [3]:

$$\begin{aligned}\bar{\sigma}^{(3)}_{xxxx}(\omega_0, E_F, 0) &\approx \frac{17G(2|E_F|, \hbar\omega_0 + i\Gamma) - 64G(2|E_F|, 2\hbar\omega_0 + i\Gamma) + 45G(2|E_F|, 3\hbar\omega_0 + i\Gamma)}{24(\hbar\omega_0)^4} \\ &+ \frac{\Gamma}{6(\hbar\omega_0)^4}\left\{17\left[\frac{1}{2|E_F| + 3\hbar\omega_0 + i\Gamma} + \frac{1}{2|E_F| - 3\hbar\omega_0 - i\Gamma}\right]\right. \\ &- 8\left[\frac{1}{2|E_F| + 2\hbar\omega_0 + i\Gamma} + \frac{1}{2|E_F| - 2\hbar\omega_0 - i\Gamma}\right] \\ &+ \left.3\hbar\omega_0\left[\frac{1}{(2|E_F| + 3\hbar\omega_0 + i\Gamma)^2} - \frac{1}{(2|E_F| - 3\hbar\omega_0 - i\Gamma)^2}\right]\right\}. \end{aligned} \tag{S38}$$

Note that ($\approx$) is because we assume $\Gamma \ll \hbar\omega_0$ [3]. Supplementary Fig.4 shows that a finite $\tau$ has a small effect on THGE for most of SLGs in literature, including the samples used in this paper.

### S2.4 $\mathbf{T}_e$ and $\mathbf{E}_\mathrm{F}$ effects on THGE

The $T_e$ and $E_F$ dependence of THGE for SLG on $SiO_2$ at $\hbar\omega_0 = 500$meV is shown in Supplementary Supplementary Fig.5, where 3 logarithmic singularities at $2|E_F| = \hbar\omega_0, 2\hbar\omega_0, 3\hbar\omega_0$ for $T_e$=0K can be seen. By increasing $T_e$, the first peak at $2|E_F| = \hbar\omega_0$ disappears and the two others merge and form a broad maximum, roughly located at $2|E_\mathrm{F}| \sim (2+3)\hbar\omega_0/2 = 2.5\hbar\omega_0$. THGE is almost insensitive to $E_\mathrm{F}$ for $2|E_\mathrm{F}| < \hbar\omega_0$. This can be explained using the asymptotic relation of the TH conductivity for $|E_\mathrm{F}| \ll \hbar\omega_0$. For $T_\mathrm{e} = 0$:

$$\sigma^{(3)}_{xxxx} \approx \frac{e^4\hbar v_\mathrm{F}^2}{(\hbar\omega_0)^4}\left\{\frac{1}{96} + \frac{i}{\pi}\left(\frac{2|E_\mathrm{F}|}{3\hbar\omega_0}\right)^3 + \dots\right\} \tag{S39}$$

Eq.S39 and Eq.2 of the main text explain the flat part of the curves in Supplementary Fig.5 in the low-doping regime ($\hbar\omega_0 > 2|E_F|$).

In order to quantify the tunability of THG in SLG by altering $E_F$, we define a parameter:

$$\xi^\mathrm{THG} \equiv \frac{\eta^\mathrm{THG}_\mathrm{max}}{\eta^\mathrm{THG}_\mathrm{min}}, \tag{S40}$$

where $\eta^{THG}_{min}$ stands for THGE in the nearly undoped regime ($|E_F| \ll \hbar\omega_0$). Supplementary Fig.6 indicates that $\xi^{THG}$ decreases by increasing $T_e$.

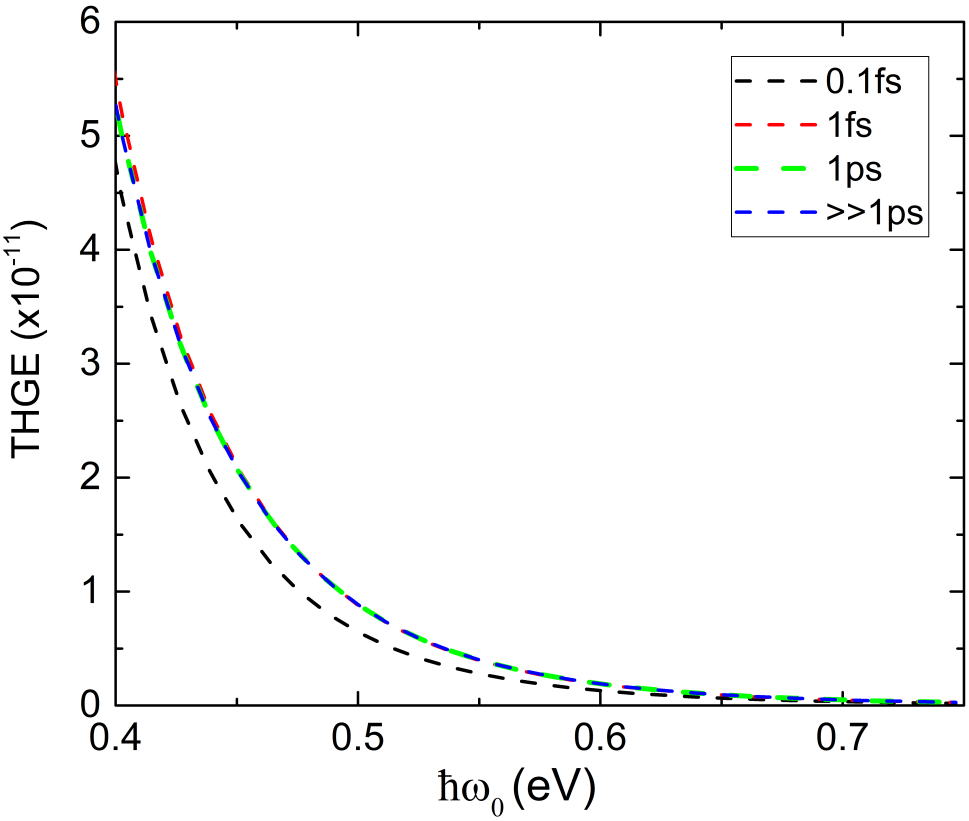


Supplementary Fig. 4. **Effect of momentum relaxation time on THGE.** THGE for SLG on Sa as a function of $\omega_0$ for different $\tau = \hbar/\Gamma$ at $T_e$=2000K and $E_F$=200meV, for incident intensity$\sim 2.4 \times 10^{12} W m^{-2}$, corresponding to the value used in our experiments

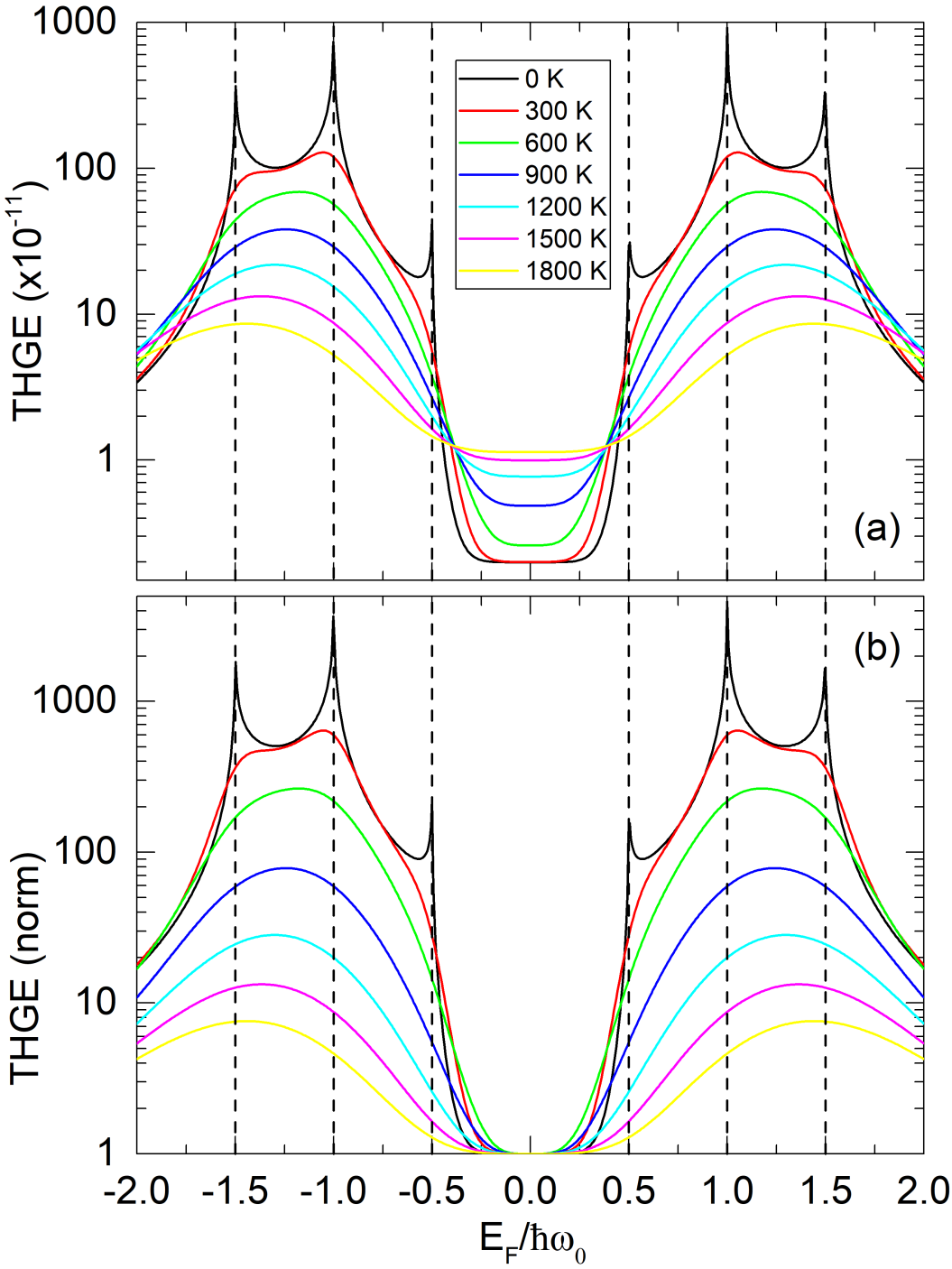


Supplementary Fig. 5. **Doping dependence of THGE at different $T_e$.** $E_F$ dependence of THGE for SLG on $SiO_2$ at $\hbar\omega_0 = 500$meV for different $T_e$ between 0K and 1800K. (a) Absolute THGE. (b) THGE normalized to the minimum so that THGE at $E_F = 0$ is equal to 1 for all $T_e$.

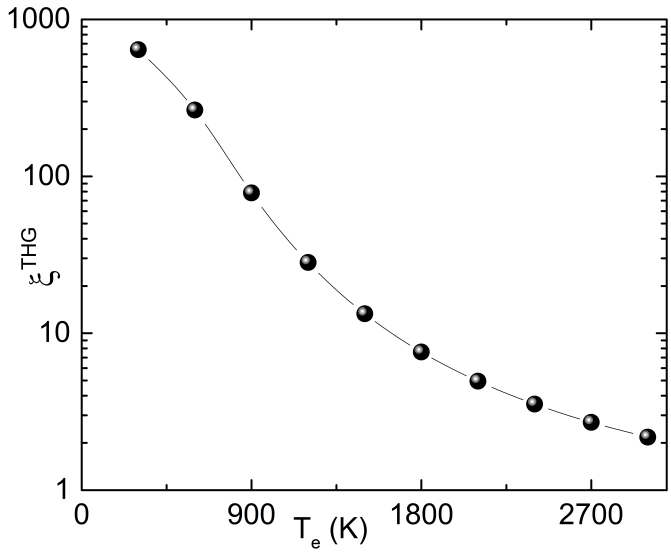


Supplementary Fig. 6. **$\mathbf{T}_e$ dependence of $\xi^{\mathrm{THG}}$.** $T_e$ dependence of doping induced enhancement parameter $\xi^{\mathrm{THG}}$ for $\hbar\omega_0 = 500$meV.

## S3 Fermi energy, Fermi level, chemical potential and electronic heat capacity in SLG

When a pulsed laser interacts with SLG, after an initial transient of a few tens fs, the electron and hole distributions in the conduction and valence bands are given by the Fermi-Dirac functions $f_{FD}(\varepsilon; \mu_\lambda, T_e)$ with the same $T_e$ and two chemical potentials $\mu_v$ and $\mu_c$ (see e.g. Refs.9–11). The chemical potential of the electrons and holes in the valence band are, by definition, opposite to each other.

At equilibrium, when $\mu_c = \mu_v$, they are denoted by $\mu$. The term Fermi level ($E_{FL}$) is also sometimes used in literature to denote $\mu$. The Fermi energy ($E_F$) is defined as the value of $\mu$ at $T_e = 0K$ [12]. $E_F$ is thus a function of the electron density only. After recombination of the photoexcited electron-hole pairs, a single Fermi-Dirac distribution is established in both bands and the equilibrium condition $\mu_v = \mu_c$ holds [9–11]. The recombination time depends on carrier density and laser fluence, and can be much longer than the time$\lesssim 20fs$ needed for thermalization (see Ref.9 and references therein).

The electronic heat capacity $c_v$ is defined as the derivative of the electronic energy density $U$ with respect to $T_e$ [12]. It depends on all the variables which affect the electronic energy density, such as $T_e$ and the carrier density or, equivalently, $\mu$ [12]. In a photoexcited system, in general, $c_v$ depends on both the electron and hole densities, i.e. on both $\mu_c$ and $\mu_v$. In this case, $c_v$

can be written as [12]:

$$c_{\mathrm{v}}(\mu_{\mathrm{c}}, \mu_{\mathrm{v}}, T_{\mathrm{e}}) = \frac{\partial}{\partial T_{\mathrm{e}}} \int_0^\infty d\varepsilon \nu(\varepsilon) \varepsilon f_{\mathrm{FD}}(\varepsilon; \mu_{\mathrm{c}}, T_{\mathrm{e}}) + \frac{\partial}{\partial T_{\mathrm{e}}} \int_0^\infty d\varepsilon \nu(\varepsilon) \varepsilon f_{\mathrm{FD}}(\varepsilon; -\mu_{\mathrm{v}}, T_{\mathrm{e}}) \ , \tag{S41}$$

where the first integral is the electron and the second the hole contribution. The density of electronic states per unit of area is $\nu(\varepsilon) = N_f|\varepsilon|/[2\pi(\hbar v_F)^2]$, with $N_f = 4$ the product of spin and valley degeneracy. The Fermi-Dirac distribution is:

$$f_{\mathrm{FD}}(\varepsilon; \mu, T_{\mathrm{e}}) = \frac{1}{e^{(\varepsilon-\mu)/(k_{\mathrm{B}}T_{\mathrm{e}})} + 1} \ . \tag{S42}$$

To take the derivative with respect to $T_e$ in Eq.S41, the dependence of $c_v$ on $T_e$ has to be specified. The electron and hole densities are given by:

$$n_{\mathrm{e}}(\mu_{\mathrm{c}}, T_{\mathrm{e}}) = \int_0^\infty d\varepsilon \nu(\varepsilon) f_{\mathrm{FD}}(\varepsilon; \mu_{\mathrm{c}}, T_{\mathrm{e}}),$$
$$n_{\mathrm{h}}(-\mu_{\mathrm{v}}, T_{\mathrm{e}}) = \int_0^\infty d\varepsilon \nu(\varepsilon) f_{\mathrm{FD}}(\varepsilon; -\mu_{\mathrm{v}}, T_{\mathrm{e}}) \ . \tag{S43}$$

Since the total electron density in both bands is constant, the difference between electron and hole densities is constant:

$$n_{\mathrm{e}}^{(0)} - n_{\mathrm{h}}^{(0)} = n_{\mathrm{e}}(\mu_{\mathrm{c}}, T_{\mathrm{e}}) - n_{\mathrm{h}}(-\mu_{\mathrm{v}}, T_{\mathrm{e}}) \ , \tag{S44}$$

where $n_e^{(0)}$ and $n_h^{(0)}$ are the intrinsic electron and hole densities before the pump. At equilibrium, when $\mu_c = \mu_v = \mu$, Eq.S44 can be solved for $\mu$. A photoexcited density $\delta n_{\mathrm{e}}$ changes the densities in both bands as follows:

$$n_{\mathrm{e}}(\mu_{\mathrm{c}}, T_{\mathrm{e}}) = n_{\mathrm{e}}(\mu, T_{\mathrm{e}}) + \delta n_{\mathrm{e}},$$
$$n_{\mathrm{h}}(-\mu_{\mathrm{v}}, T_{\mathrm{e}}) = n_{\mathrm{h}}(-\mu, T_{\mathrm{e}}) + \delta n_{\mathrm{e}} \ . \tag{S45}$$

After finding $\mu$ with Eq.S44, one can get $\mu_c$ and $\mu_v$ with Eq.S45. This defines the dependence of $c_v$ on $T_e$ in Eq.S41, and allows us to calculate the derivative with respect to the temperature. The result of Eq.S41 is shown in Supplementary Fig.7 for $\mu_c = \mu_v = \mu$. In Ref.13 the following expression is given for $c_{\mathrm{v}}$:

$$c_{\mathrm{v}}(T_{\mathrm{e}}) = \frac{18\zeta(3)}{\pi(\hbar v_{\mathrm{F}})^2} k_{\mathrm{B}}^3 T_{\mathrm{e}}^2 \ . \tag{S46}$$

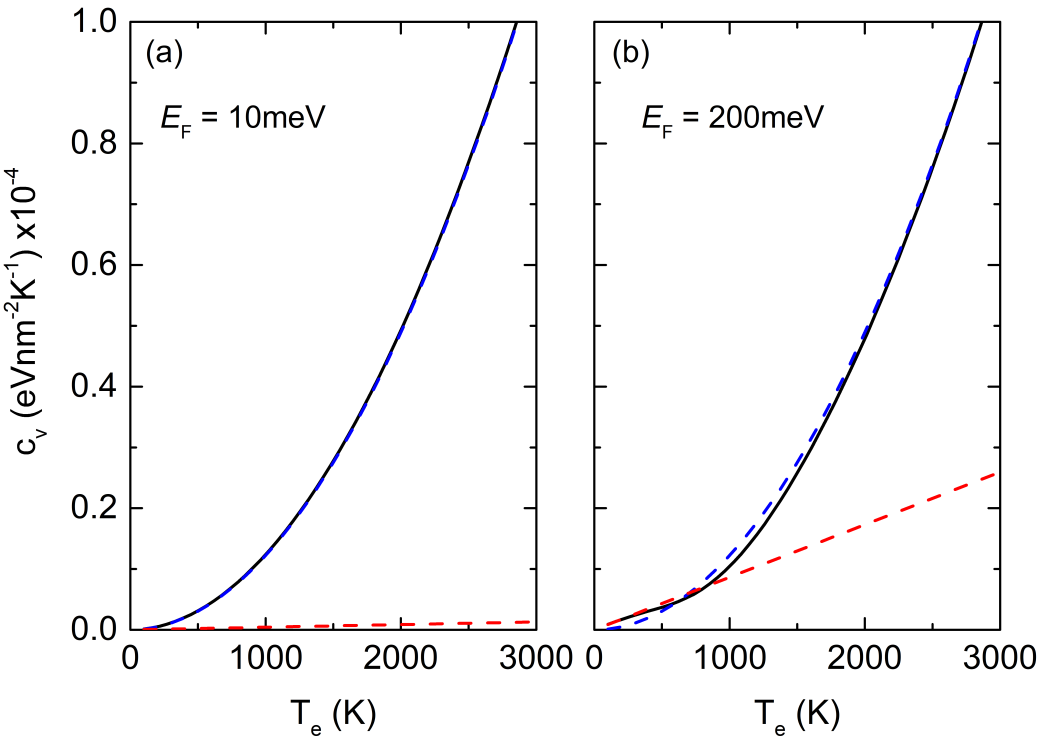


Supplementary Fig. 7. **$T_e$ dependence of the $c_v$ in equilibrium conditions.** Calculations for (a) $E_F$=10 and (b) 300meV. The blue and red dashed lines are Eqs.S46, S47.

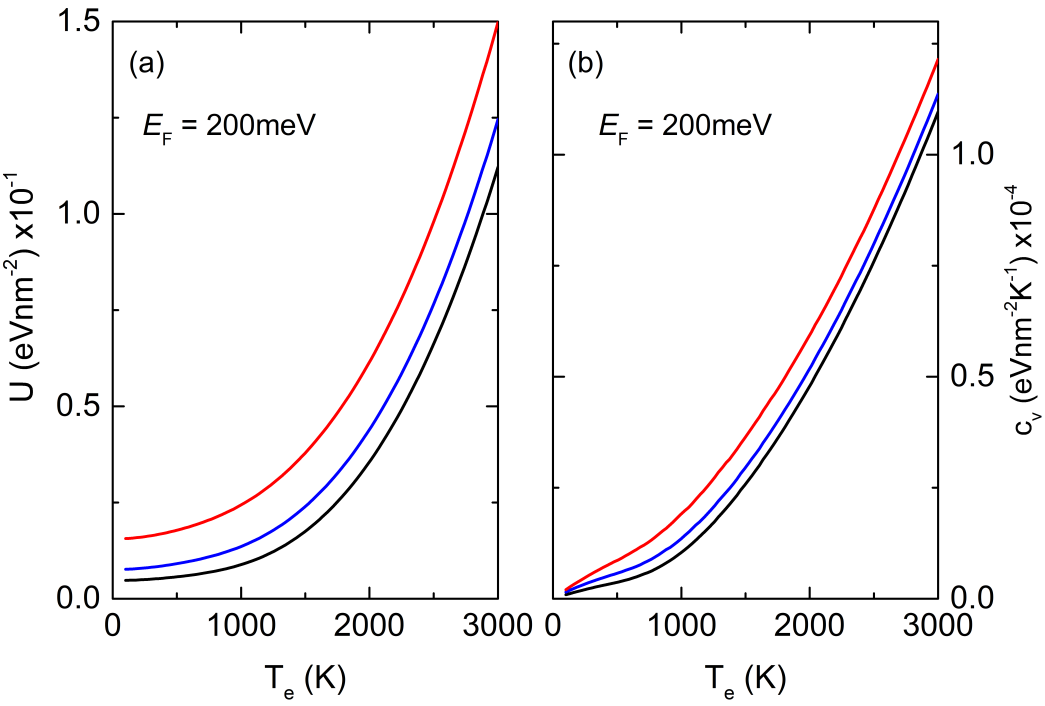


Supplementary Fig. 8. **$\mathbf{T}_e$ dependence of the electron energy density and $\mathbf{c}_v$ in out of equilibrium conditions.** (a) Electron energy density and (b) $c_v$ for $E_F$=200meV. The blue, and red lines correspond to photoexcited densities $\delta n_e = 10^{12}$ and $3{\times}10^{12} cm^{-2}$, while the black line corresponds to a thermalized system with a single $\mu$

In principle, as noted in Ref.14, Eq.S46 is valid at the charge neutrality point $|\mu| \ll k_B T$ only. For a degenerate system, $k_B T \ll |\mu|$, we have [4]:

$$c_{\rm v}(\mu, T_{\rm e}) = \frac{\pi^2}{3}\nu(E_{\rm F})k_{\rm B}^2 T_{\rm e} \ , \tag{S47}$$

as derived *e.g.* in Eqs.8.10 of Ref.4, in Eq.4 of Ref.15 and in Eq.8 in the Supplementary Information of Ref.16. However, the numerical calculation in Supplementary Fig.7 shows that the quadratic approximation (Eq.S46) is much better in the regime where $T_e \sim 1000K$ and $\mu \sim 100$meV. Supplementary Fig.8 shows that, taking into account the difference between $\mu_c$ and $\mu_v$, for typical values of the photoexcited density, contributes$\gtrsim$ 15% to $c_v$.

## S4 Absorption coefficient and estimate of steady-state $T_e$ under pumping and dissipation

### S4.1 SLG absorption coefficient

The average absorbed power per unit area in SLG excited by a pulse of duration $\Delta t$, fluence $\mathcal{F}$, and average frequency of the photons $\omega/2\pi$ can be written as:

$$\frac{P}{A} = \mathcal{P}[\alpha(\omega, \mu_{\rm c}, \mu_{\rm v}, T_e)]\frac{\mathcal{F}}{\Delta t} \ , \tag{S48}$$

where $\alpha(\omega, \mu_{\rm c}, \mu_{\rm v}, T_e)$ is the absorption coefficient and the function $\mathcal{P}(x) = x\,\theta(x)$ equals $x$ for $x > 0$ and 0 for $x < 0$. For simplicity we omit $\mathcal{P}$ in the main text. For frequencies in the optical domain, we consider only the contributions due to direct vertical inter-band electronic transitions. The origin of these transitions is purely quantum and does not depend on disorder. On the other hand, intra-band transitions are mediated by defects [18] and can be described classically. In general, the absorption coefficient is a function of the electron distribution:

$$\alpha(\omega; \mu_{\rm c}, \mu_{\rm v}, T_e) = (2.3\%)\frac{2}{1+n_{\rm sub}}\left[1 - f_{\rm FD}(\hbar\omega/2; \mu_{\rm c}, T_e) - f_{\rm FD}(\hbar\omega/2; -\mu_{\rm v}, T_e)\right] \ , \tag{S49}$$

for a sample lying between air and a substrate with refractive index $n_{\rm sub}$. This expression is obtained using Eq.7.34 in Ref. [19] for the real part of the inter-band conductivity and the relation between absorption and conductivity of thin films discussed in Ref. [20]. This means that the absorption is reduced due to Pauli blocking if the electron or hole distributions at $E_F = \hbar\omega/2$ increase. As $T_e$ increases, the absorption becomes a sizable fraction of its maximum value 2.3%, even in the frequency range $\hbar\omega < 2E_F$ where it vanishes at room temperature.

### S4.2 Estimate of steady-state $T_e$ under pumping and dissipation

The number of photoexcited electron-hole pairs per unit area in the time interval $dt$ is given by the number of absorbed photons in the same time interval per unit area, i.e. $(dn_{\rm e} + dn_{\rm h})/2 = (P/A)/(\hbar\omega_0)dt$. In the steady state, the energy delivered by the pump is transferred into the phonon modes. Hence, we identify the electron-hole recombination time with $\tau$. We then get:

$$\begin{aligned}\frac{1}{2}\left(\frac{dn_{\rm e}}{dt} + \frac{dn_{\rm h}}{dt}\right) &= \frac{1}{\hbar\omega_0}\frac{P}{A} \\ &- \frac{1}{2}\frac{[n_{\rm e}(\mu_{\rm c}, T_{\rm e}) + n_{\rm h}(-\mu_{\rm v}, T_{\rm e})] - (n_{\rm e}^{(0)} + n_{\rm h}^{(0)})}{\tau} \ .\end{aligned} \tag{S50}$$

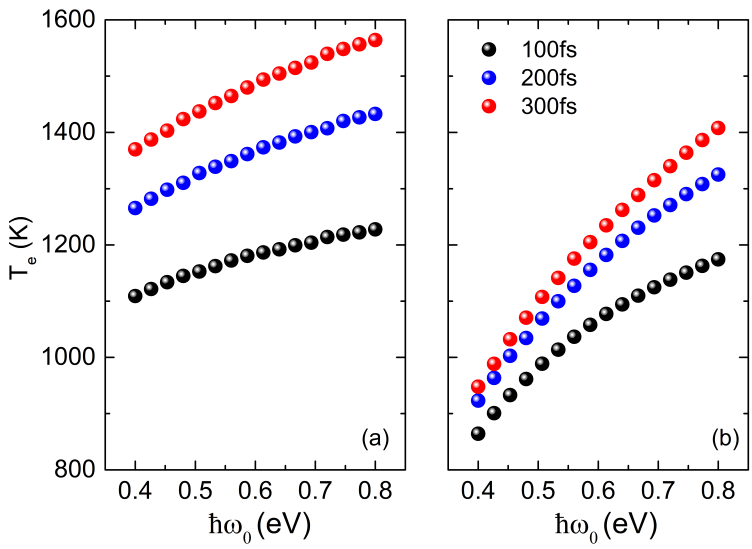


Supplementary Fig. 9. $\hbar\omega_0$ **dependence of $\mathbf{T}_e$ in photoexcited SLG**. $T_e$ as a function of $\hbar\omega_0$ for $E_F$=200meV and $\tau$=100 (black), 200 (blue), and 300fs (red). In (a) we use a constant $\alpha$=(2.3%)/[(1 + $n_{\rm sub}$)/2] while in (b) we use the full functional dependence of Eq.S49.

In the steady state this becomes:

$$n_{\rm e}^{(0)} + n_{\rm h}^{(0)} = n_{\rm e}(\mu_{\rm c}, T_{\rm e}) + n_{\rm h}(-\mu_{\rm v}, T_{\rm e}) - \frac{2\tau}{\hbar\omega_0}\frac{P}{A}. \tag{S51}$$

Combining Eqs.S44,S51, we find:

$$\delta n_{\rm e} = \frac{\tau}{\hbar\omega_0}\frac{P}{A}\ . \tag{S52}$$

To calculate $E_F$ (e.g. for a $n$-doped sample) one needs to solve Eqs.S42, S43, S44 with $\mu_{\rm c} = \mu_{\rm v} = E_F$, $T_e = 0$, and $n_h^{(0)} = 0$, finding $E_F = \hbar v_F\sqrt{\pi n_e}$. This relation can be used at $T_e = 300K$ and electron densities $n_{\rm e}^{(0)} \gtrsim 10^{11}$ because the density of thermally excited holes is negligible. In photoexcited SLG, even after recombination of the photoexcited electron-hole pairs, the $T_e$ dependence of $\mu$ cannot be ignored. In this case, to calculate $\mu$, one needs to solve Eqs.S42,S43, S44 with $\mu_{\rm c} = \mu_{\rm v} = \mu$ and $n_{\rm h}^{(0)} = 0$ as a function of $T_e$. This gives $\mu = E_F[1 - \pi^2 T_{\rm e}^2/(6T_{\rm F}^2)]$ for $T_e \lesssim T_{\rm F}$ and $\mu = E_F T_F/(4\ln 2 \times T_{\rm e})$ for $T_e \gtrsim T_{\rm F}$ [17], where $T_{\rm F} = E_{\rm F}/K_{\rm B}$, with $K_{\rm B}$ the Boltzmann constant. For a typical case of $E_F$=200meV and $T_e$ =1500K, we have $\mu \sim 0.3 - 0.5E_F$. To calculate $T_e$, we solve the non-linear Eq.4 in the main text, with the $T_e$ dependence of $\alpha$ and $c_v$ discussed above. The values of $T_e$, as a function of $\hbar\omega_0$, for

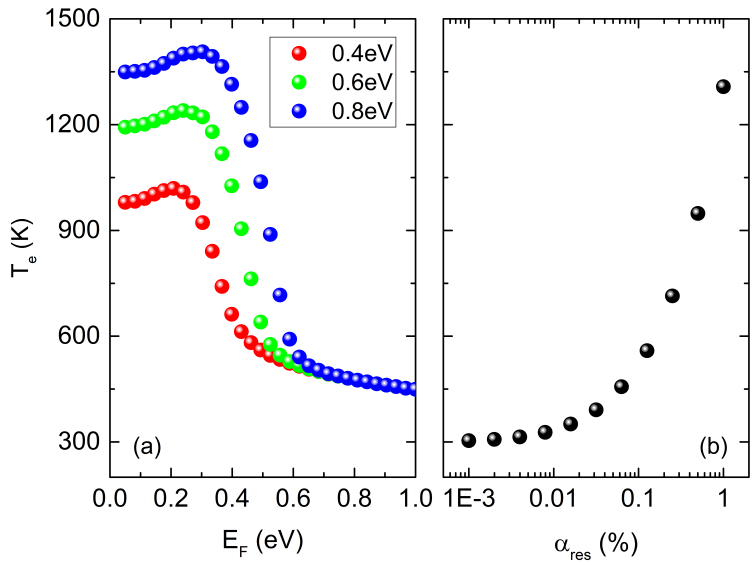


Supplementary Fig. 10. **$E_F$ dependence of $T_e$ in photoexcited SLG**. (a) Steady-state $T_e$ as a function of equilibrium $E_F$ for $\tau$=200fs and $\hbar\omega_0$=0.4 (red), 0.6 (green) and 0.8eV (blue). (b) $T_e$ as a function of residual (intra-band) absorption for $E_F$=0.6eV and $\hbar\omega_0$=0.4eV.

several $\tau$ and the experimental conditions used in this paper ($\mathcal{F}$=70.0$\mu$J/cm$^2$, $\Delta t$=300fs, $n_{sub}$=1.44), are in Supplementary Fig.9. $T_e$ increases for higher energy photons and longer $\tau$. $T_e$ ranges between$\simeq$800 and 1500K.

For $T_e$ >300K inter-band transitions can occur also when $\hbar\omega_0 < 2E_F$, as show in Eq.S49. To apply the theory also to lower temperatures, where intra-band transitions due to disorder play a role in the absorption process, we modify Eq.4 of the main text as follows:

$$T = T_0 + \tau \frac{\mathcal{P}[\alpha(\omega;\mu_{\rm c},\mu_{\rm v},T) + \alpha_{\rm res}]}{c_{\rm v}(\mu_{\rm c},\mu_{\rm v},T)} \frac{\mathcal{F}}{\Delta t} \ , \tag{S53}$$

where a constant $\alpha_{\rm res}$ is added to $\alpha(\omega,\mu_{\rm c},\mu_{\rm v},T_e)$ to take into account the contribution of the residual (intra-band) absorption. No modifications are needed in Eq.S51 because the residual absorption, stemming from intra-band transitions, does not directly affect the photoexcited density. We assume that distinct contributions to the absorption are additive because $\alpha$ is much smaller than unity. Supplementary Fig.10a plots $T_e$ as a function of $E_F$ for $\tau$=200fs, $\alpha_{res}$=0.1% and different $\hbar\omega_0$. Supplementary Fig.10b shows $T_e$ for different $\alpha_{res}$ for $E_F$=0.6eV and $\hbar\omega_0$=0.4eV. Very small values of $\alpha_{res} \sim 0.1\%$, corresponding to $\alpha \sim 2.3\%/20$, lead to $T_e$ ~500-600K. $T_e$ rapidly increases to>1000K for $\alpha_{res}$ ~1%.

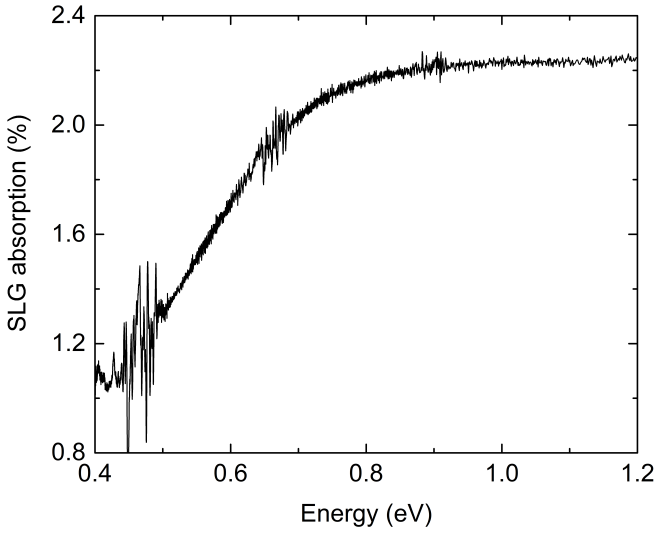


Supplementary Fig. 11. **SLG absorption**. Absorption spectrum on the SLG on Sa sample. The measurement was performed in transmission geometry with a Cary 600 Series FTIR Spectrometer.

Supplementary Fig.11 reports the experimental absorption for the SLG on Sa sample ($E_F$ ∼250meV). $\alpha_{res}$ at $\hbar\omega < 2E_F$ is∼1%. Since intra-band absorption is mediated by defects [18] and $n_D$ is∼2-3 times higher in SLG on Sa compared to SLG on $Si/SiO_2$, we use 0.1% for $\alpha_{res}$ in Supplementary Fig.10a.

# References


[1] Mikhailov, S. A. Quantum theory of the third-order nonlinear electrodynamic effects of graphene. *Phys. Rev. B* **93,** 085403 (2016).

[2] Rostami, H. & Polini, M. Theory of third-harmonic generation in graphene: A diagrammatic approach. *Phys. Rev. B* **93,** 161411 (2016).

[3] Cheng, J. L., Vermeulen, N. & Sipe, J. E. Third-order nonlinearity of graphene: Effects of phenomenological relaxation and finite temperature. *Phys. Rev. B* **91,** 235320 (2015);

[4] Giuliani, G. F. & Vignale, G. *Quantum Theory of the Electron Liquid* (Cambridge University Press, Cambridge, 2005).

[5] Shen, Y. R. Optical Second Harmonic Generation at Interfaces. *Annu. Rev. Phys. Chem.* **40,** 327 (1989).

[6] Merano, M. Nonlinear optical response of a two-dimensional atomic crystal. *Opt. Lett.* **41,** 187 (2016).

[7] Boyd, R. W. *Nonlinear Optics* (Academic Press, London, 2008).

[8] Jackson, J. D. *Classical Electrodynamics* (John Wiley & Sons, New York, 1998).

[9] Tomadin, A., Brida, D., Cerullo, G., Ferrari, A. C. & Polini, M. Nonequilibrium dynamics of photoexcited electrons in graphene: Collinear scattering, Auger processes, and the impact of screening. *Phys. Rev. B* **88,** 035430 (2013).

[10] Malic, E., Winzer, T., Bobkin, E., & Knorr, A. Microscopic theory of absorption and ultrafast many-particle kinetics in graphene. *Phys. Rev. B* **84,** 205406 (2011).

[11] Sun, B. Y., Zhou, Y., & Wu, M. W. Dynamics of photoexcited carriers in graphene. *Phys. Rev. B* **85,** 125413 (2012).

[12] Grosso, G. & Pastori Parravicini, G. *Solid State Physics* (Academic Press, Oxford, 2000).

[13] Lui, C. H., Mak, K. F., Shan, J. & Heinz, T. F. Ultrafast Photoluminescence from Graphene. *Phys. Rev. Lett.* **105,** 127404 (2010).

[14] Sun, D. *et al.* Ultrafast hot-carrier-dominated photocurrent in graphene. *Nat. Nanotech.* **7**, 114 (2012).

[15] Low, T., Perebeinos, V., Kim, R., Freitag, M. & Avouris, P. Cooling of photoexcited carriers in graphene by internal and substrate phonons. *Phys. Rev. B* **86,** 045413 (2012).

[16] Tielrooij, K. J. *et al.* Photoexcitation cascade and multiple hot-carrier generation in graphene. *Nat. Phys.* **9,** 248 (2013).

[17] Hwang, E. H. & Das Sarma, S. Screening-induced temperature-dependent transport in two-dimensional graphene. *Phys. Rev. B* **79,** 165404 (2009).

[18] Mak, K. F., Ju, L., Wang, F. & Heinz, T. F. Optical spectroscopy of graphene: From the far infrared to the ultraviolet. *Solid State Commun.* **152,** 1341 (2012).

[19] Katsnelson, M.I. *Graphene* (Cambridge University Press, Cambridge, 2012).

[20] Tinkham, M. Energy Gap Interpretation of Experiments on Infrared Transmission through Superconducting Films. *Phys. Rev.* **104,** 845 (1956).